Received: 14 February 2017 | Revised: 15 May 2017 | Accepted: 17 May 2017

DOI: 10.1111/ter.12275

PAPER

WILEY Terra Nova

# A novel nuclear forensic tool involving deposit type normalized rare earth element signatures

Tyler L. Spano[1] | Antonio Simonetti[1] | Thomas Wheeler[1] | Grace Carpenter[1] | Devonee Freet[1] | Enrica Balboni[1,2] | Corinne Dorais[1] | Peter C. Burns[1,3]

[1]Department of Civil and Environmental Engineering and Earth Sciences, University of Notre Dame, Notre Dame, IN, USA

[2]Glenn T. Seaborg Institute, Physical and Life Science Directorate, Lawrence Livermore National Laboratory, Livermore, CA, USA

[3]Department of Chemistry and Biochemistry, University of Notre Dame, Notre Dame, IN, USA

**Correspondence**
Tyler L. Spano, Department of Civil and Environmental Engineering and Earth Sciences, University of Notre Dame, Notre Dame, IN, USA.
Email: tspanofr@nd.edu

**Funding information**
Department of Homeland Security Domestic Nuclear Detection Office Academic Research Initiative, Grant/Award Number: DHS-14-DN-077-ARI-01

## Abstract

Identifying the provenance of uranium-rich materials is a critical objective of nuclear forensic analysis. Rare earth element (REE) distributions within uranium ores are well-established forensic indicators, but quantifying and correlating trace element signatures for U ores to known deposits has thus far involved intricate statistical analyses. This study reports average chondrite normalized (CN)-REE signatures for important U deposit types worldwide, which are then employed to evaluate U ore paragenesis using a simple linear regression analysis. This technique provides a straightforward method that can aid in determining the deposit type of U ores based on their REE abundances, and combined with other forensic indicators (e.g. radiogenic isotope signatures) can provide essential provenance information for nuclear materials.

## 1 | INTRODUCTION

Uranium ores are the essential raw material used for nuclear fuel and are characterized by a diverse range of compositions resulting from varied geological origins (Cuney, 2008; Dahlkamp, 1993; Fayek, 2013; IAEA 2009; Table 1). The age of U ore deposits spans from Archaean to Quaternary, and they may result from processes occurring under geochemical conditions ranging from high-temperature magmatic to low-temperature surficial (Cuney, 2008). The International Atomic Energy Agency (IAEA) delineates 15 unique U deposit types, and each is characterized by various subdivisions (Hore-Lacy, 2016). Numerous studies have investigated rare earth element (REE) signatures of U ores from diverse origins, and these are indeed effective provenance indicators when normalized to chondritic abundances (e.g. Alexandre, Kyser, Layton-Matthews, Joy, & Uvarova, 2015; Bonhoure, Kister, Cuney, & Deloule, 2007; Boulyga, Konegger-Kappel, Richter, & Sangely, 2015; Fleischer & Altschuler, 1969; Frimmel, Schedel, & Brätz, 2014; Mayer, Wallenius, & Ray, 2005; Mercadier et al., 2011).

Comparison of chondrite normalized (CN)-REE signatures for source attribution as applied to nuclear forensics has been largely qualitative and, when quantitative, only expressed as a function of intricate statistical analyses (e.g. Principal Component Analysis-PCA; Alexandre et al., 2015; Keegan et al., 2008). Qualitatively, the shapes of CN-REE patterns are compared to gain insight into the origin of U-rich materials including uranium ores, ore concentrates (UOC) and other derivative materials (e.g. uranium peroxide, ammonium diuranate and uranyl nitrate) relevant to the front end of the nuclear fuel cycle (Frimmel et al., 2014; Mercadier et al., 2011; Varga et al., 2017). Here, we propose a simplified system for determining the origin (i.e. U deposit type) of potentially intercepted nuclear material.

## 2 | URANINITE

The most abundant U-bearing ore mineral is uraninite (ideally $UO_2$, but more commonly $(U^{4+}_{1-x-y-z-u}U^{6+}_{x}REE^{3+}_{y}M^{2+}_{z}\square^{4-}_{u})O_{2+x-0.5y-z-2u}$, where $M^{2+}$ and $\square$ indicate divalent metals and a vacant site

  

**TABLE 1** Summary of uranium deposit types, subtypes and ore/accessory minerals

| Deposit type and subtypes | Host environment/mode of mineralization | Ore and accessory minerals |
|---|---|---|
| **Intrusive**<br>Anatectic<br>Plutonic | Differentiated ore bodies related to anatectic or plutonic activity.<br>**Alaskite** type intrusive deposits occur as large stocks and domes to tabular dikes and small lenses of coarse-grained leucogranites.<br>**Quartz-monzonite** deposits are highly differentiated and, in some cases, consist of several stages of magmatic activity.<br>**Carbonatite** intrusive deposits are highly differentiated and related to alkaline volcanism.<br>**Peralkaline syenite** deposits are contained within domes and stocks and generally consist of refractive U phases.<br>**Pegmatite** U deposits are related to late stage magmatism and often occur as tabular to lenticular dikes, swells and apophyses. | U minerals include uraninite, thoriferous uraninite, uranothorianite, uranothorite and other refractory U minerals. Hexavalent U minerals may be present in locally weathered zones. Monazite, apatite, zircon, metallic sulphides and halite are often found in Alaskite-hosted and quartz-monzonite U. Metallic sulphides are commonly associated with carbonatite-related intrusive U. |
| **Granite Related**<br>Endogranitic<br>Perigranitic | Veins within granitic to episyenitic bodies occur as lens- or sheet-like disseminations, fracture in-fillings, stockworks in deformed rocks and/or as shear zones in regionally metamorphosed terranes.<br>**Endogranitic** deposits occur within granite as linear ore bodies as veins/stockworks or as disseminations in episyenite bodies.<br>**Perigranitic** deposits are located in country rock, commonly sedimentary to metasedimentary units, adjacent to granite. | U occurs as uraninite, pitchblende, coffinite and alteration products thereof. U is associated with metallic sulphides, silicates, fluorite, barite and calcite. |
| **Polymetallic Iron-Oxide Breccia Complex**[a] | U ore occurs within hematite-rich granitic to metasedimentary–metavolcanic breccias. | Low grade U in the form of pitchblende, coffinite and/or brannerite is often associated with Cu–Au–Ag and rare earth elements. |
| **Volcanic Related**[a]<br>Structure-bound<br>Strata-bound<br>Volcano-sedimentary | Occur near or within volcanic calderas. Host rocks range from mafic to felsic and often include pyroclastics and/or intercalated clastic sediments. Mineralization may span several stratigraphic levels. U may occupy intrusions or occur as disseminations in structure-bound and strata-bound deposits, respectively. | U occurs as pitchblende, coffinite, secondary (hexavalent) phases and occasionally as brannerite. Gangue minerals include fluorite, barite, quartz and carbonates. |
| **Metasomatite**[a]<br>Na-metasomatite<br>K-metasomatite<br>Skarn | Deposits are contained within continental shields and median masses in which orogenic belts have undergone intense metasomatism related to deep fault systems. U ores result from complex, multistage paragenesis. Granites, migmatites, gneisses and quartzite may host metasomatic U deposits. | Uraninite, pitchblende, coffinite, uranothorianite, uranothorite, thorite, hexavalent U minerals, brannerite and other U-titanate phases are common ores in metasomatite deposits. Allanite, bastnaesite, monazite, xenotime and zircon are often associated with U. Gangue minerals include metallic sulphides, calcite and hematite. |
| **Metamorphite**<br>Strata-bound<br>Structure-bound<br>Marble-hosted | Deposits occur as impregnations, veins, disseminations and shear zones with metamorphic rocks unrelated to granitic intrusions. Metamorphite deposits are often hosted within mafic metasediments and are often metamorphosed to amphibolite grade facies. | U occurs as uraninite, pitchblende, coffinite and locally as hexavalent U minerals. Sulphides, selenides and arsenides may be present as accessory phases. |
| **Proterozoic Unconformity**<br>Unconformity-contact<br>Basement-hosted<br>Stratiform fracture-controlled | Occur above, below or along unconformable contacts between Archaean to Palaeoproterozic crystalline basement rocks and siliciclastic sedimentary rocks of Proterozoic age. Deposits may be intensely altered by lateritic weathering and/or hydrothermal activity. Tectonic deformation results in ore-forming fluid redistribution.<br>**Basement hosted** (fracture-bound) deposits are located directly below the unconformable contact.<br>**Unconformity hosted** (clay-bound) deposits occur within overlying sedimentary cover of unconformity.<br>**Stratiform fracture-controlled** U occurs within clastic sediments and faults intersecting basement rocks and overlying sediments. | U primarily occurs as pitchblende and occasional uraninite. Quartz, carbonates, metallic sulphides and clay minerals are often in association with U minerals. |
| **Collapse Breccia Pipe**[a] | U is hosted within lithological fragments in vertical, cylindrical breccia pipes often resulting from karst dissolution and alteration. | U as pitchblende accompanied by numerous metallic oxides, carbonates and sulphates. |

(Continues)

**TABLE 1** (Continued)

| Deposit type and subtypes | Host environment/mode of mineralization | Ore and accessory minerals |
|---|---|---|
| **Sandstone**<br>Basal Channel<br>Tabular<br>Roll-Front<br>Tectonic-lithologic<br>Mafic dykes/sills | Occur within continental fluvial or marginal marine sedimentary settings.<br>**Basal channel** deposits are palaeodrainage systems characterized by sequences of alluvial–fluvial sediments where U is associated with detrital plant debris in ribbon-like configurations.<br>**Tabular-peneconcordant** deposits occur as irregular lenses and lenticular masses within reduced sediments and organic matter. These deposits are related to detrital carbonaceous debris emplaced either contemporaneously or via redistribution following initial deposition of host sandstones.<br>**Roll-front** deposits result when oxidizing fluids remobilize U along a hydrologic gradient. Precipitation occurs when mobilized U encounters a reducing front. These deposits display diffuse boundaries with reduced sandstone convex down to the hydrologic gradient.<br>**Tectonic-lithologic** U deposits are thick ore bodies located within fault zones and adjacent sandstone beds discordant to surrounding strata and are often associated with detrital plant material.<br>**Mafic dykes/sills** are characterized by mineralization along lithological contacts which may be concordant or crosscut with respect to Proterozoic sandstones. | U as pitchblende, coffinite, uraniferous humate. Hexavalent U minerals (predominantly, uranyl phosphates and vanadates) occur in oxidized locations. Metallic sulphides, hematite, calcite and native selenium are common accessory phases in sandstone deposits. |
| **Palaeo-Quartz Pebble Conglomerate**[a]<br>U-dominant<br>Au-Dominant | Detrital U is deposited as basal units or as intraformational conglomerates and may be modified by diagenetic processes. | U and/or Th oxides occur with pyrite, gold and accessory metallic oxide and sulphide minerals. |
| **Surficial**[b]<br>Peat-bog<br>Fluvial valley<br>Lacustrine-playa<br>Pedogenic/fracture filled | Occur as Tertiary to Recent deposits where U is concentrated in sediments, soils or proximal to/within uraniferous source rocks. Calcretes, lacustrine-playa deposits, heavily weathered U-rich granites and, less commonly, peat bogs host surficial U deposits. | Surficial deposits contain hexavalent U minerals almost exclusively. Carnotite and uranyl vanadates are the predominant U ores minerals. |
| **Lignite–Coal**[b]<br>Stratiform<br>Fracture-controlled | U occurs in lignite and/or coal mixed with silt and/or clay or adjacent to carbonaceous mud and silt/sandstone beds. Lignite–coal deposits are composed of high percentages of land plant debris and coalified detritus. | U adsorbed to carbonaceous matter or bound to inorganic compounds. Metallic trace elements may be present. |
| **Carbonate**[b]<br>Strata-bound<br>Cataclastic<br>Palaeokarst | Carbonate related U deposits occur in limestone and dolostone as syngenetic and strata-bound or as structure-related ore bodies within folds, faults, fractures or karst formations. | Pitchblende, coffinite and U–Si–Ti phases. Metallic sulphides, silicates and phosphates occur as accessory phases. |
| **Phosphate**[b]<br>Organic phosphorite<br>Phosphorite<br>Continental phosphorite | Phosphate U deposits are largely contained within marine phosphorite originating from continental-shelves. Synsedimentary, stratiform, disseminated U occurs in fine-grained apatite. | Predominant U phase is cryptocrystalline fluor-carbonate apatite, with minor or absent discrete primary U minerals. Al and Ca–Al phosphate minerals may be present. |
| **Black Shale**[a]<br>Stratiform<br>Stockwork | U occurs in marine, organic-rich shale and as coal-rich pyritic shale characterized by synsedimentary, disseminated U adsorbed to organic materials. | U adsorbed to organic material and clay particles. Minor hexavalent U minerals may be present. |

[a]Deposits of this type have been integrated with other deposits due to geochemical similarities. See Table 3.
[b]Deposits are not discussed in detail in this work. Modified from Dahlkamp (1993), IAEA (2009, 2016), Hore-Lacy (2016), Cuney and Kyser (2015), Cui, Yang, and Samson (2012), Finch (1996), Rai, Zakaulla, and Chaki (2009) and Plant, Simpson, Smith, and Windley (1999).

respectively) (Finch & Murakami, 1999; Janeczek & Ewing, 1992). As evidenced by the complex stoichiometry of uraninite, Th, REEs, divalent elements (Pb, Ca, etc.) and U of higher oxidation states are often incorporated within its crystal structure during initial crystallization and/or diagenesis (Plasil, 2014). Preferential hosting of elements is largely based upon similarities in ionic radii, with elements approximating the 1Å radius of $U^{4+}$ in eightfold-coordination being favoured, which results in enrichments of $Th^{4+}$ (1.05Å) and/or REEs (1.16–0.98Å; Finch & Murakami, 1999).

**TABLE 2** List of uranium deposits included in deposit type average chondrite normalized rare earth element signatures

| Locality | Country | Reference | Analysis type |
|---|---|---|---|
| Intrusive | | | |
| Rossing | Namibia | Mercadier et al. (2011) | SIMS[a] |
| Luthi, Nummi Pusula | Finland | Mercadier et al. (2011) | SIMS[a] |
| Moore Lake, Athabasca Basin | Canada | Mercadier et al. (2011) | SIMS[a] |
| Kola Peninsula | Russia | Mercadier et al. (2011) | SIMS[a] |
| Yancy, Spruce Pine District | NC, USA | Balboni, Jones, Spano, Simonetti, & Burns (2016) | LA-ICP-MS |
| Ruggles Pegmatite | NH, USA | Balboni et al. (2016) | LA-ICP-MS |
| Mitchell | NC, USA | Alexandre et al. (2015) | LA-ICP-MS |
| Roode Pegmatite | Norway | Alexandre et al. (2015) | LA-ICP-MS |
| Vaal Reef, Witwatersrand Basin | South Africa | Depiné et al. (2013) | LA-ICP-MS |
| Granite related | | | |
| Boirs Noirs, Massif Central | France | Frimmel et al. (2014) | LA-ICP-MS |
| Commanderie | France | Frimmel et al. (2014) | LA-ICP-MS |
| Ecarpiere | France | Frimmel et al. (2014) | LA-ICP-MS |
| Jachymov | Czech Republic | Frimmel et al. (2014) | LA-ICP-MS |
| Kowary | Poland | Frimmel et al. (2014) | ICP-MS[b] |
| Jadugua | India | Pal, Chaudhuri, McFarlane, Mukherjee, & Sarangi (2011) | LA-ICP-MS |
| Schneeberg | Germany | Alexandre et al. (2015) | LA-ICP-MS |
| Pribam | Czech Republic | Alexandre et al. (2015) | LA-ICP-MS |
| Ranwick | ON, Canada | Alexandre et al. (2015) | LA-ICP-MS |
| Central Ukraine U Province | Ukraine | Cuney et al. (2012) | ICP-MS[b] |
| Illimaussaq | Greenland | Sørrensen (1992) | XRF[c] |
| Prominent Hill | Australia | Forbes, Giles, Freeman, Sawyer, & Normington (2015) | EMP[c] |
| Olympic Dam | Australia | Ciobanu, Wade, Cook, Schmidt Mumm, & Giles (2013) | LA-ICP-MS |
| Nolans Bore | Australia | Huston et al. (2016) | ICP-MS[b] |
| Camry, Theano Point | ON, Canada | Alexandre et al. (2015) | LA-ICP-MS |
| Metamorphite | | | |
| Kawanga | Zambia | Mercadier et al. (2011) | SIMS[a] |
| Mistamisk | QC, Canada | Mercadier et al. (2011) | SIMS[a] |
| Mary Kathleen, Selwyn Range | Australia | Frimmel et al. (2014) | LA-ICP-MS |
| Igarapé, Carajás Cu-Au Belt | Brazil | Tallarico et al. (2005) | LA-ICP-MS[c] |
| Tirschenreuth | Germany | Frimmel et al. (2014) | LA-ICP-MS |
| Talvivaara | Finland | Lecomte et al. (2014) | LA-ICP-MS |
| Luiswishi, Lufilian Belt | Democratic Republic of the Congo | Eglinger et al. (2013)) | LA-ICP-MS |
| Malundwe, Lufilian Belt | Zambia | Eglinger et al. (2013) | LA-ICP-MS |
| Mitukuluku, Lufilian Belt | Zambia | Eglinger et al. (2013) | LA-ICP-MS |
| Dorrmorsbach | Germany | Frimmel et al. (2014) | LA-ICP-MS |
| Orphan Lode | AZ, USA | Balboni et al. (2016) | LA-ICP-MS |
| Marshall Pass | CO, USA | Balboni et al. (2016) | LA-ICP-MS |
| Echo Bay | NWT, Canada | Alexandre et al. (2015) | LA-ICP-MS |
| Great Bear Lake, Athabasca Basin | Canada | Alexandre et al. (2015) | LA-ICP-MS |
| Port Radium | NWT, Canada | Alexandre et al. (2015) | LA-ICP-MS |
| Wittichen, Black Forest Region | Germany | Frimmel et al. (2011) | LA-ICP-MS |

(Continues)

**TABLE 2** (Continued)

| Locality | Country | Reference | Analysis type |
|---|---|---|---|
| Shinkolobwe, Lufilian Belt | Democratic Republic of the Congo | Eglinger et al. (2013) | LA-ICP-MS |
| Kolwezi, Lufilian Belt | Democratic Republic of the Congo | Eglinger et al. (2013) | LA-ICP-MS |
| Nkana, Lufilian Belt | Democratic Republic of the Congo | Eglinger et al. (2013) | LA-ICP-MS |
| Kalongwe, Lufilian Belt | Democratic Republic of the Congo | Eglinger et al. (2013) | LA-ICP-MS |
| Swambo, Lufilian Belt | Democratic Republic of the Congo | Eglinger et al. (2013) | LA-ICP-MS |
| Unconformity related | | | |
| Eagle Point, Athabasca Basin | Canada | Mercadier et al. (2011) | SIMS[a] |
| Millennium, Athabasca Basin | Canada | Mercadier et al. (2011) | SIMS[a] |
| Nabarlek, Kombolgie Basin | Australia | Mercadier et al. (2011) | SIMS[a] |
| Koongarra, Kombolgie Basin | Australia | Mercadier et al. (2011) | SIMS[a] |
| Cigar Lake, Athabasca Basin | Canada | Mercadier et al. (2011) | SIMS[a] |
| Sue, Athabasca Basin | Canada | Mercadier et al. (2011) | SIMS[a] |
| McArthur River, Athabasca Basin | Canada | Mercadier et al. (2011) | SIMS[a] |
| Collins Bay, Athabasca Basin | Canada | Fryer & Taylor (1987) | XRF |
| Pine Creek Geosyncline | Australia | Fryer & Taylor (1987) | XRF |
| Centennial, Athabasca Basin | Canada | Alexandre et al. (2015) | LA-ICP-MS |
| Maurice Bay, Athabasca Basin | Canada | Alexandre et al. (2015) | LA-ICP-MS |
| Ranger | Australia | Fisher, Cleverley, Pownceby, & MacRae (2013) | ICP-OES[b], ICP-MS[b] |
| Sandstone | | | |
| Chu-Sarysu Basin | Kazakhstan | Mercadier et al. (2011) | LA-ICP-MS |
| Powder River Basin | WY, United States | Balboni et al. (2016) | LA-ICP-MS |
| Ike | UT, United States | Alexandre et al. (2015) | LA-ICP-MS |
| Three Crows | NE, United States | Leibold (2013) | LA-ICP-MS |
| Dulann Uul | Mongolia | Lach, Mercadier, Dubessy, Boiron, & Cuney (2013) | LA-ICP-MS |
| Beverley | Australia | Wülser, Brugger, Foden, & Pfeifer (2011) | LA-ICP-MS |
| Sandstone-Tabular | | | |
| Happy Jack | UT, USA | Balboni et al. (2016) | LA-ICP-MS |
| Monument Valley | UT, USA | Balboni et al. (2016) | LA-ICP-MS |
| Black Hawk | NM, USA | Alexandre et al. (2015) | LA-ICP-MS |
| Wood Lode, Lisbon Valley Anticline | UT/CO, USA | Alexandre et al. (2015) | LA-ICP-MS |

SIMS, secondary ion mass spectrometry; (LA)-ICP-MS, laser ablation inductively coupled plasma mass spectrometry; XRF, X-ray fluorescence spectroscopy; EMP, electron microprobe; ICP-OES, inductively coupled plasma optical emission spectrometry.
All other trace element data obtained from uraninite.
[a]Gd and Yb concentrations calculated from: Gd = 1/3 Sm + 2/3 Tb and Yb = 1/2 Tm + 1/2 Lu.
[b]Bulk (whole-rock) analysis.
[c]Monazite analysis.

Observed partitioning of REEs in U oxides appears to be strongly dependent on temperature, fluid chemistry and element availability (hypogene REE source), and thus these elements have been used extensively as forensic indicators (e.g. Fayek, 2013; Frimmel et al., 2014; Keegan, Wallenius, Mayer, Varga, & Rasmussen, 2012; Keegan et al., 2014; Mayer, Wallenius, & Fanghänel, 2007; Mayer, Wallenius, & Varga, 2015; Mercadier et al., 2011). At high temperatures, particularly above 350°C, incorporation mechanisms that discriminate against available cations based upon size are negated due to the dilational nature of the uraninite structure; this results in a relatively flat CN-REE pattern (Mercadier et al., 2011). A negative Eu anomaly may also be observed at elevated temperatures, which results from substitution for Ca by Eu during early crystal fractionation of plagioclase in silicate melts (Gao & Wedepohl, 1995). When crystallization temperatures for uraninite drop below 350°C, differentiation of REEs results from constraints imposed by the uraninite structure. This feature favours elements having comparable ionic radii to $U^{4+}$, leading to an enrichment in the mid-REEs (MREEs), Tb–Er (Mercadier et al., 2011). In sedimentary U deposits, trace element incorporation is influenced by

**TABLE 3** Reassigned deposits

| Deposit name and locality | Deposit type | New assignment | Reason for reassignment |
|---|---|---|---|
| Jaduguda, India | Metamorphite | Granite related | The Singhbhum granite is the main geochemical source of U in this area. CN-DTA-REE analysis indicates a granitic origin (Mazumder, 2005; Pal et al., 2011). |
| Prominent Hill Olympic Dam Nolans Bore, Australia | Polymetallic Iron-Oxide Breccia Complex | Granite related | The Olympic Dam iron-oxide copper gold and related deposits are contained entirely within the Roxby Down syenogranite (Ciobanu et al., 2013; Johnson & McCulloch, 1995; Oreskes & Einaudi, 1990). |
| Central Ukraine U Province, Ukraine | Metasomatite | Granite related | U deposits in the Central Ukraine U Province developed in felsic rocks and range from nearly unaltered granites to highly albitized areas resulting from Na-metasomatism and calcite–biotite replacement of minerals during K-metasomatism (Cuney et al., 2012). |
| Vaal Reef, Witwatersrand Basin, South Africa | Palaeo-Quartz Pebble Conglomerate | Intrusive | The palaeoplacer Witwatersrand basin U-deposit is included with intrusive deposits due the highly differentiated plutonic-felsic hypogene U source (Depiné et al., 2013). |
| Mary Kathleen, Selwyn Range, Australia | Metasomatite | Metamorphite | Although a skarn origin (and resulting metasomatic deposit assignment) was initially suggested, a younger age found to coincide with regional metamorphism warrants inclusion with metamorphite deposits (Frimmel et al., 2014). |
| Igarapé, Carajás Cu–Au Belt, Brazil | Polymetallic Iron-Oxide Breccia Complex | Metamorphite | Igarapé is hosted by hydrothermally altered metavolcanic-sedimentry breccias (Tallarico et al., 2005). |
| Tirschenreuth, Germany | Granite Related | Metamorphite | Tirschenreuth U occurs within high-grade metapelites in proximity to Variscan basement rocks (Frimmel et al., 2014). |
| Talvivaara, Finland | Black Shale | Metamorphite | U deposited as a by-product of metamorphism of black schists during the Svecofennian orogeny (Lecomte et al., 2014). |
| Orphan Lode, United States | Collapse Breccia Pipe | Metamorphite | Host rock alteration via pyritization, dolomitization, cacitization, silicification, desilification and/or Mg depletion are characteristic of this deposit (Dahlkamp, 1990). |
| Dorrmorsbach | Intrusive | Metamorphite | U is hosted within the contact between fine-grained pegmatite and biotite schist (Frimmel et al., 2014). CN-DTA-REE analysis indicates ore chemistry associated with metamorphic origin. |

precipitation of insoluble U mineral phases, adsorption of U to organic phases, secondary oxides and clays, and the ability of U to substitute for other elements with similar physiochemical properties (Dahlkamp, 1993).

## 3 | METHODS

In this study, intrusive, granite-related, metamorphite, unconformity and sandstone-related deposits are discussed in detail (Table 1). Sandstone U deposits are the most numerous, with >600 recognized deposits worldwide and with a corresponding increased availability of REE data. The number of identified granite-related (160), unconformity (107), metamorphite (96) and intrusive (88) deposits has also provided a significant amount of available information and has permitted their inclusion in this study (IAEA 2016).

Extensive literature and database searches were conducted to collect trace element data for each deposit type of interest, resulting in a dataset of 67 U deposits (total number of analyses = 532). The locality, country of origin and source of REE data for each deposit included in the database employed here are described in Table 2 and shown in Figure 1. Due to geochemical similarities and/or unclear ore origins for some U deposits, they have been included with other types as described in Table 3. After collection of trace element data, REE concentrations (ppm) were normalized to chondritic abundances (McDonough & Sun, 1995). Chondrite normalized (CN)-REE values within a single dataset were then added to determine total CN-REE content (ΣCN-REE). CN values for each REE in a dataset were then divided by ΣCN-REE to obtain values that are normalized to total REE content, or fractions of 1. This calculation ensures that each locality included in a deposit type average (DTA) contributes equally to the signature; differences in absolute concentration are negated, and relative abundances of REEs prevail (Figure 2). Figure S1 illustrates the DTA patterns with associated uncertainties (1$\sigma$ *SD*) based on the range of REE concentrations reported for each deposit type. The REE budget within U ores is in part controlled by the presence of accessory mineral phases such as monazite and xenotime. DTA analysis is therefore most efficient for U ores exhibiting an equigranular, homogenous texture (e.g. magmatic) as opposed to those of sedimentary origin.

A U-rich material of unknown origin can then be compared with each deposit type by plotting CN-REE data for an unknown as a function of the DTA-CN-REE signatures provided here (Table 4). A linear correlation with a slope closest to unity is observed when the geochemical origin of the unknown is similar to that of a corresponding deposit type (Figures 3–5). The degree of similarity can be

**TABLE 4** Deposit type average chondrite normalized rare earth element signatures and associated uncertainties (1σ). Graphical representation of DTA-CN-REE signatures and associated uncertainties is available in Figure S1

| | Intrusive $n = 50$ | | Granite $n = 222$ | | Metamorphite $n = 157$ | | Unconformity $n = 40$ | | Sandstone $n = 50$ | | Sandstone (Tabular) $n = 13$ | |
|---|---|---|---|---|---|---|---|---|---|---|---|---|
| | DTA | 1σ | DTA | 1σ | DTA | 1σ | DTA | 1σ | DTA | 1σ | DTA | 1σ |
| La | 0.01 | 0.01 | 0.31 | 0.13 | 0.03 | 0.06 | 0.01 | 0.02 | 0.29 | 0.12 | 0.06 | 0.03 |
| Ce | 0.03 | 0.02 | 0.20 | 0.04 | 0.05 | 0.05 | 0.01 | 0.01 | 0.16 | 0.03 | 0.10 | 0.02 |
| Pr | 0.05 | 0.03 | 0.14 | 0.03 | 0.08 | 0.09 | 0.01 | 0.01 | 0.11 | 0.02 | 0.11 | 0.02 |
| Nd | 0.05 | 0.03 | 0.11 | 0.03 | 0.07 | 0.05 | 0.02 | 0.01 | 0.08 | 0.02 | 0.11 | 0.03 |
| Sm | 0.12 | 0.05 | 0.06 | 0.03 | 0.13 | 0.05 | 0.06 | 0.03 | 0.05 | 0.02 | 0.09 | 0.02 |
| Eu | 0.02 | 0.02 | 0.02 | 0.01 | 0.09 | 0.06 | 0.06 | 0.02 | 0.03 | 0.02 | 0.09 | 0.05 |
| Gd | 0.08 | 0.05 | 0.04 | 0.02 | 0.11 | 0.04 | 0.06 | 0.04 | 0.04 | 0.02 | 0.06 | 0.01 |
| Tb | 0.15 | 0.06 | 0.03 | 0.01 | 0.12 | 0.05 | 0.20 | 0.04 | 0.04 | 0.02 | 0.06 | 0.02 |
| Dy | 0.14 | 0.05 | 0.02 | 0.01 | 0.09 | 0.04 | 0.21 | 0.04 | 0.04 | 0.02 | 0.06 | 0.01 |
| Ho | 0.11 | 0.04 | 0.02 | 0.01 | 0.07 | 0.03 | 0.11 | 0.06 | 0.04 | 0.02 | 0.06 | 0.01 |
| Er | 0.09 | 0.04 | 0.02 | 0.01 | 0.05 | 0.02 | 0.10 | 0.02 | 0.03 | 0.02 | 0.05 | 0.01 |
| Tm | 0.08 | 0.05 | 0.01 | 0.01 | 0.04 | 0.02 | 0.06 | 0.03 | 0.03 | 0.01 | 0.05 | 0.02 |
| Yb | 0.04 | 0.03 | 0.01 | 0.01 | 0.04 | 0.03 | 0.04 | 0.03 | 0.03 | 0.01 | 0.06 | 0.03 |
| Lu | 0.03 | 0.02 | 0.01 | 0.01 | 0.03 | 0.02 | 0.04 | 0.03 | 0.03 | 0.01 | 0.05 | 0.03 |

quantified, as the slope and correlation coefficient of linear regression both approach one (in the ideal case) when the unknown corroborates with a given deposit type. Subsequent to the compilation of signatures, this method was validated by treating 12 REE datasets for uraninite and UOC from deposits of known origin as "unknowns". In all cases, the deposit type could be positively identified.

## 4 | INTRUSIVE

Intrusive U deposits consist of differentiated ore bodies related to anatexis or plutonic activity, and despite resulting from unique petrogenic processes, all are considered as one group here (Table 1). The quartz-pebble conglomerate deposits of the palaeoplacer Witwatersrand basin in South Africa are also included due to similar hypogene U sources (Table 3; Depiné, Frimmel, Emsbo, Koenig, & Kern, 2013). The DTA-REE signature of intrusive deposits displays a convex pattern characterized by LREE and HREE depletions and a prominent negative Eu anomaly (Figure 2a). Crystallographic control resulting in preferential incorporation of REEs with ionic radii similar to that of $U^{4+}$ in eightfold coordination is evidenced by the bell-shaped pattern centred on the MREEs (Mercadier et al., 2011).

## 5 | GRANITE-RELATED

Granite-related deposits consist of U mineralization hosted within lens- or sheet-like disseminations, fracture in-fillings, as stockworks in deformed rocks and/or as shear zones within or adjacent to granite or episyenite bodies (Hore-Lacy, 2016; Roberts & Hudson, 1983). Granite-related U deposits are distinguished as a function of proximity to the granitic pluton contact (either Endogranitic or Perigranitic), and both types are considered together in this study (Table 1). The Olympic Dam iron-oxide breccia complex in Australia and related U deposits are included with granite-related vein deposits in this study (Table 3). Metamorphite deposits from Jadugua, India and metasomatite deposits of the Central Ukraine U province have also been included with granite-related U deposits (Table 3). The CN-DTA-REE signature for granite-related deposits is characterized by a negatively sloping linear trend with LREE enrichment and HREE depletion (Figure 2b) and a prominent negative Eu anomaly. This signature for granite-related deposits is heavily influenced by the availability of REEs and is similar in shape to the CN pattern for monazite (Alexandre et al., 2015).

## 6 | METAMORPHITE

Metamorphite U deposits originate from diagenetic alteration of U-rich sediments or volcanic materials. Deposits of this type develop within diverse geochemical environments and share the common characteristic of forming at elevated temperatures (350–500° C), often within synorogenic settings (Cuney, 2008; Cuney et al., 2012; Skirrow et al., 2009). Due to similarities in paragenesis for metamorphite, collapse-breccia pipe and metasomatic U deposits, these designations are combined in this study (Hore-Lacy, 2016; Table 3). Metamorphite U deposits are indicated by a convex DTA signature with depletions in the lightest and heaviest REEs (Figure 2c). The DTA-CN-REE pattern for U originating from metamorphic processes exemplifies crystallographic controls upon trace element incorporation, with favourability for REEs of similar ionic radius to $U^{4+}$ evidenced by MREE enrichment. Although qualitatively similar in shape to the signature for intrusive deposits, the DTA signature for

metamorphite deposits displays less-extreme LREE and HREE depletions and a much less pronounced Eu anomaly.

## 7 | UNCONFORMITY

Unconformity-related (UR) deposits are hosted along or above unconformable contacts between clastic red beds and crystalline basement rocks, and are typically the result of palaeoweathering and diagenetic alteration (Dahlkamp, 1993; Hore-Lacy, 2016). Although UR deposits are subdivided with respect to proximity to an unconformable boundary (Table 1), all groups are included in calculating the DTA-CN-REE signature for deposits of this type. The average signature for UR deposits exhibits depletion of light rare earth elements (LREEs) and is further characterized by enrichments in Tb and Dy (Figure 2d). LREE depletion in the DTA-CN-REE signature for unconformity deposits may be attributed to the cogenesis of LREE-rich Al-Phosphate-Sulphate minerals (Gaboreau, Cuney, Quirt, Patrier, & Mathieu, 2007).

## 8 | SANDSTONE

Sandstone-hosted U deposits are found in continental fluvial or marginal marine sedimentary environments and may be further classified by depositional, structural and geochemical distinctions (Table 1; Dahlkamp, 1993; IAEA 2009). Roll-front, basal-channel and tectonic-lithologic sandstone deposits are considered separately from tabular-peneconcordant deposits in this study. The DTA-CN-REE signatures for roll-front, basal-channel and tectonic-lithologic sandstone deposits are characterized by LREE enrichment, a negative Eu anomaly (likely an artifact of the hypogene U source) and a relatively flat heavy rare earth element (HREE) pattern (Figure 2e).

Differences in the metallogenesis of tabular sandstone deposits are evidenced by a DTA-CN-REE signature unique from those of other sandstone-related U ores (Figure 2f). Formation of tabular U deposits often involves diagenetic precipitation of U at higher temperatures than other sandstone-related deposits (Cuney, 2008). As a result, this pattern displays less REE differentiation than lower-temperature sandstone-related deposits, with slight depletions in La and Lu, no Eu anomaly and, overall, a relatively flat shape.

## 9 | DISCUSSION

### 9.1 | Method validation

REE signatures for uraninite and UOC from 12 U deposits of known origin were treated as unknowns for method validation. For example, the trace element signature of a uranium ore concentrate (UOC)

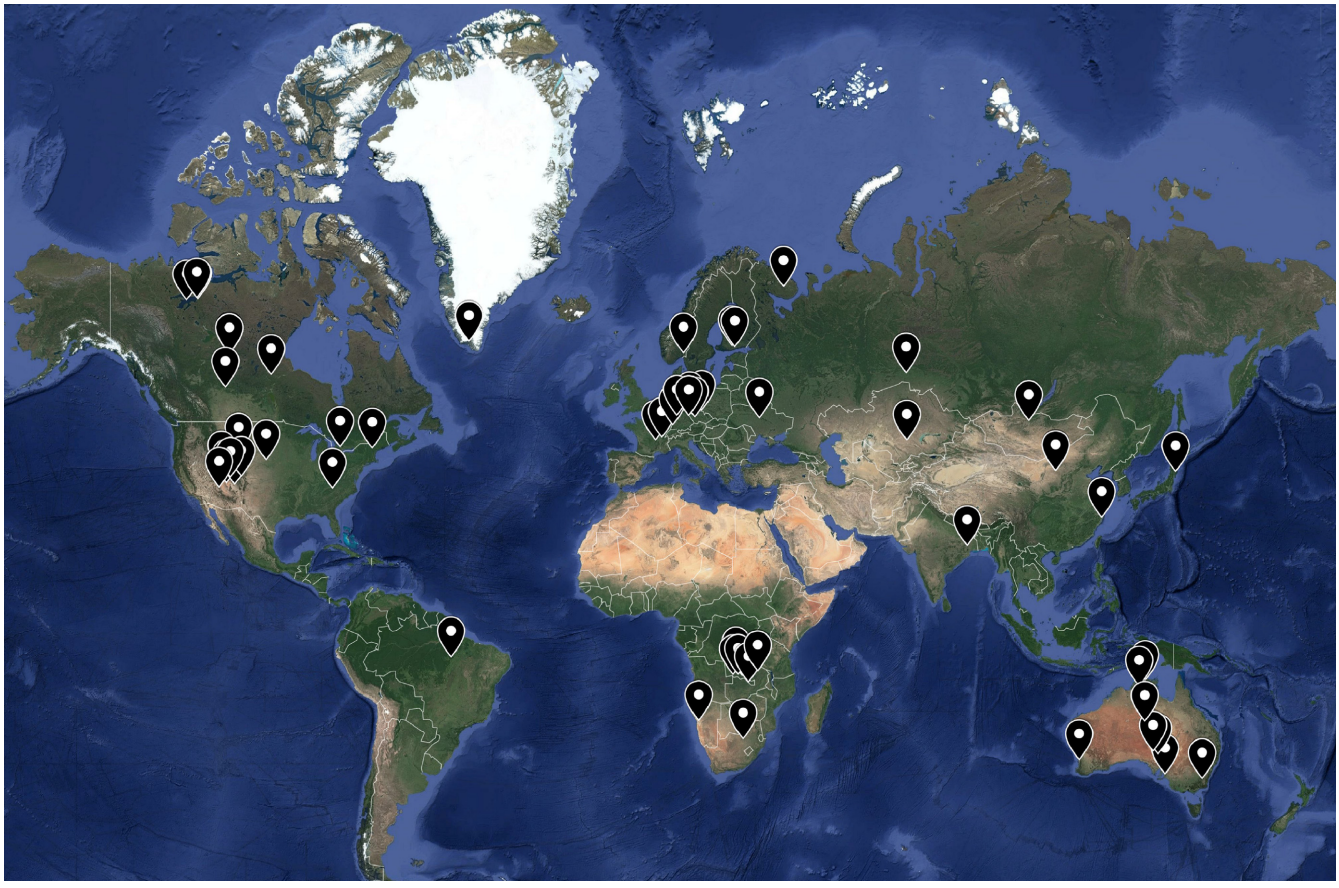

**FIGURE 1** Localities of uranium deposits included in the deposit type average chondrite normalized rare earth element signatures obtained in this study

originating from a roll-front deposit in the USA was plotted as a function of the DTA-REE signatures (Figure 3). A significant, positive correlation was observed with both roll-front type sandstone and granite-related vein deposits. The latter is expected given that the initial source of remobilized U that resulted in the roll-front deposits has been attributed to Precambrian granitic veins (Finch, 1996). Despite correlation with both granite-related and sandstone deposits, a sandstone origin is favoured as the correlation coefficients for both deposits are comparable, yet the slope of the sandstone-related deposits is closer to one. Uraninite from the North Ordos Basin in China (Zhang et al., 2017) and UOCs originating from Olympic Dam, Rossing, Rio Algom, Denison, Milliken, Anaconda, Straz and Rayrock deposits (Varga, Wallenius, & Mayer, 2010) have also been correctly identified using DTA-CN-REE analysis (Figures S2–S10).

The same method was used to determine the origin of U-rich materials from the Musoshi deposit in the Lufilian Belt of Southern Africa. Other U localities in this region were identified as metamorphite type deposits; however, a unique CN-REE signature for Musoshi indicated a distinct origin. DTA-CN-REE analysis indicates that the metallogenesis of Musoshi U most closely resembles an intrusive origin (Figure 4). This assignment corroborates the interpretations of Eglinger et al. (2013) who discussed the complexity of Lufilian-hosted U deposits.

Although classified as a roll-front type deposit by the IAEA (2016), examination of REE signatures from the Tono deposit in

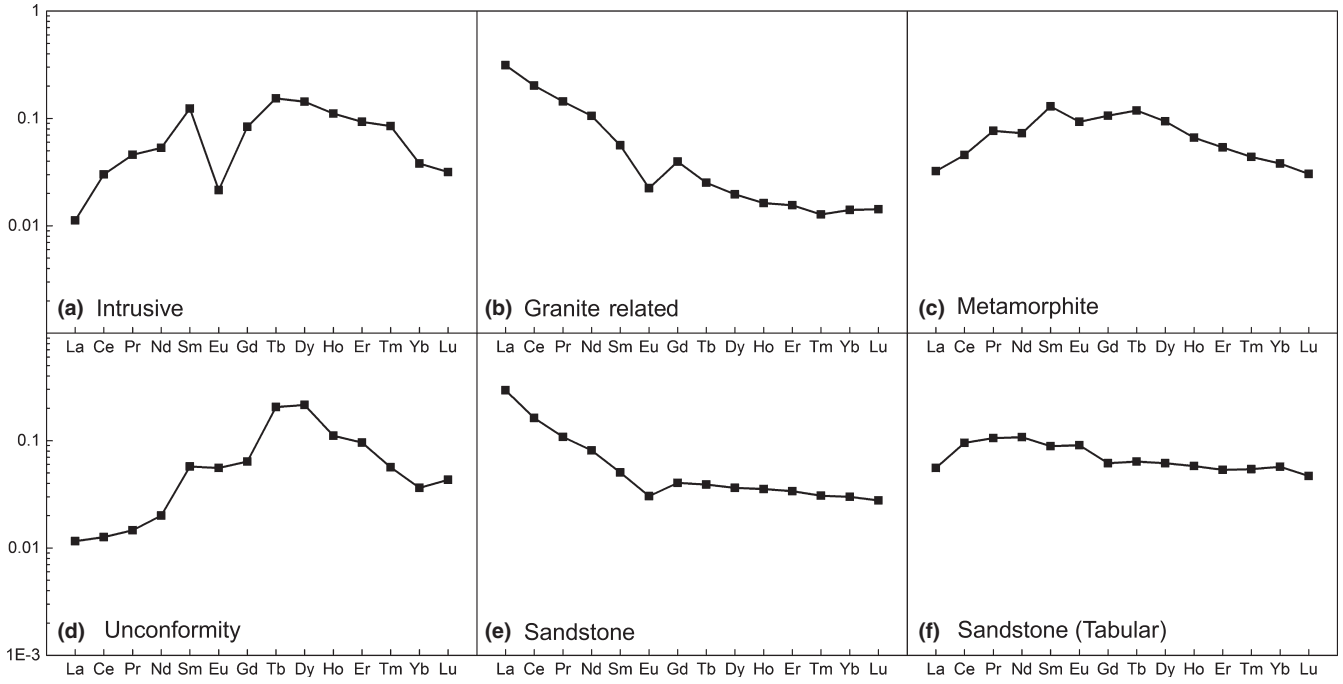


**FIGURE 2** Deposit type average chondrite normalized rare earth element signatures obtained in this study

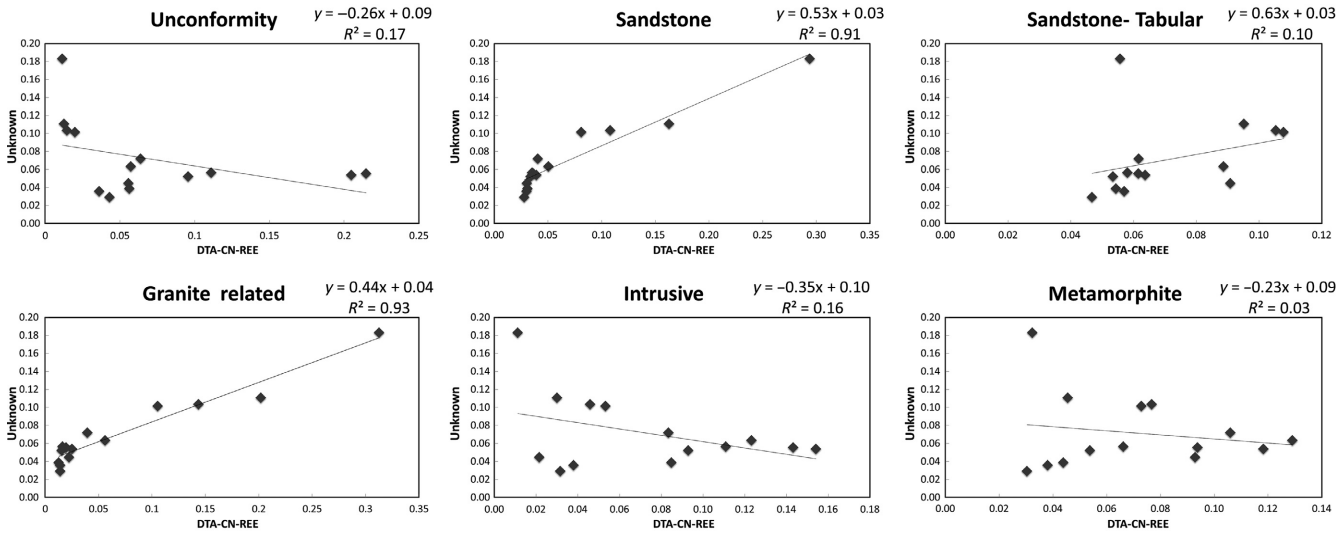


**FIGURE 3** Uranium ore concentrate from a roll-front deposit treated as an unknown and plotted as a function of DTA REE signatures. Correlations are observed with granite-related and sandstone type deposits

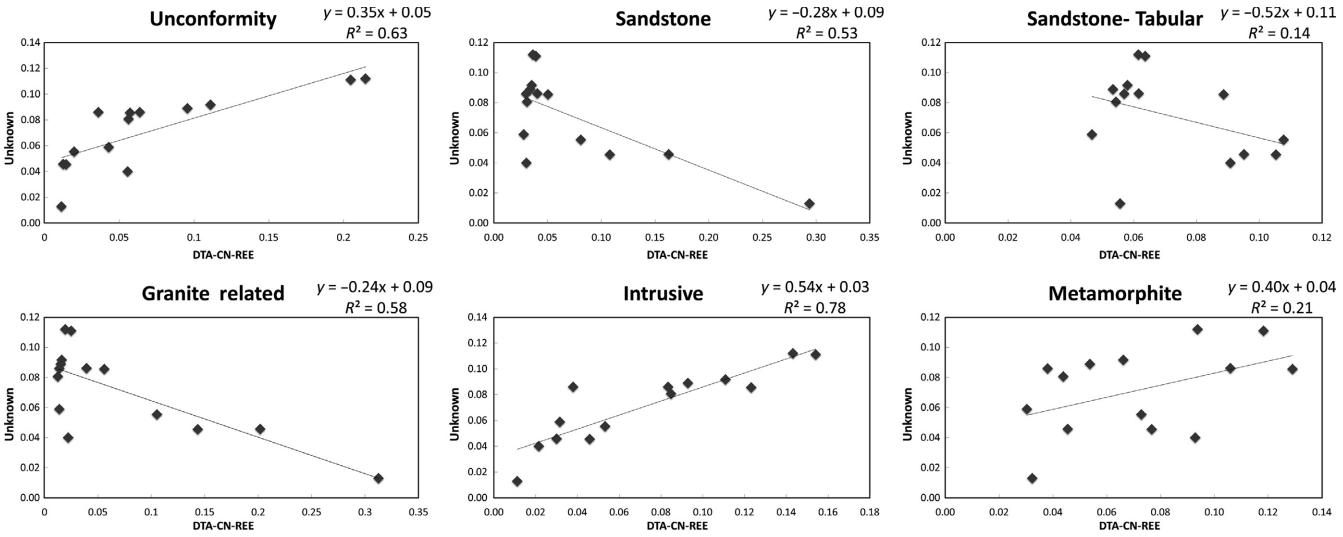


**FIGURE 4** CN-REE signature of Musoshi uraninite treated as an unknown and plotted as a function of deposit type average CN-REE signatures. Analysis reveals an intrusive origin

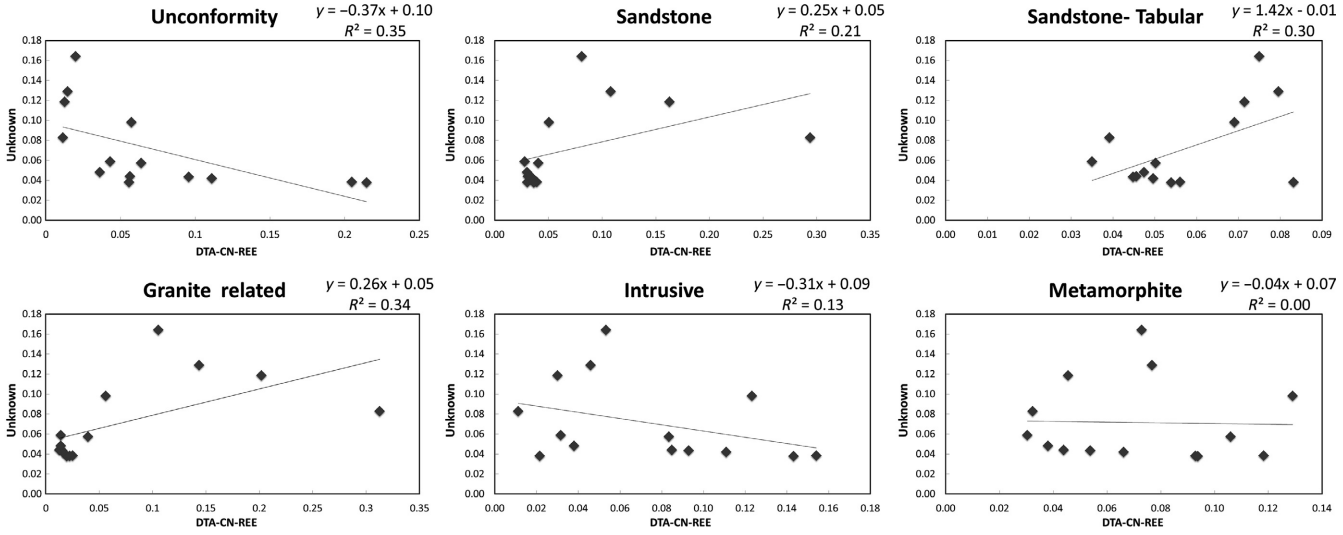


**FIGURE 5** CN-REE signature of Tono uraninite treated as an unknown and plotted as a function of DTA REE signatures. Analysis reveals that this U originates from a tabular sandstone deposit

Japan using the method reported here indicates that U in this region most likely originated from tabular sandstone deposits (Figure 5). The $R^2$ values associated with the DTA-REEs for unconformity-related (0.35), sandstone (0.21), tabular sandstone (0.30) and granite-related (0.34) deposits are relatively weak, but the slope (1.42) is clearly closer to unity for tabular sandstone deposits than for the remaining deposit types (Figure 5). The tabular sandstone paragenesis is preferred given the ore mineralogy and metallogenesis proposed by Takahashi et al. (2002), which was attributed to reducing conditions imparted by interaction with organic matter.

## 9.2 | Method limitations

It is important to note that the linear regression method developed here provides a timely and simplified evaluation of the paragenesis for U ores, but, in some instances, additional lines of evidence (e.g. field observations, petrographic information) are needed to either confirm or refute the DTA-CN-REE analysis. The greatest challenge of this work is elucidating the boundaries between similar deposit types (Cuney, 2008), and this is complicated by post-formational processes, such as alteration, erosion, diagenesis etc. Moreover, processing of U ores, in some cases, alters the geochemical signatures and may result in an incorrect assignment of a deposit type using this method (Varga et al., 2017). As a result, the nature and provenance of the U-rich material being examined must be considered when utilizing DTA-CN-REE signatures for deposit type analysis.

## 10 | CONCLUSIONS

DTA-CN-REE data provide a means to rapidly determine the deposit type of U-rich material of unknown origin, and this method is

simpler and less time-intensive to use compared with the intricacies of PCA analysis. This method also aids accurate identification and classification of U deposits with ambiguous geochemical signatures. As the number of U deposits included within this database increases, worldwide DTA-CN-REE region-specific signatures can be established, which will further assist in determining the provenance of U ores.

## ACKNOWLEDGEMENTS

Funding for this project was provided by the Department of Homeland Security Domestic Nuclear Detection Office Academic Research Initiative (DHS-14-DN-077-ARI-01). The authors also thank Stefanie Lewis for her contributions to the DTA database.

## REFERENCES

Alexandre, P., Kyser, K., Layton-Matthews, D., Joy, B., & Uvarova, Y. (2015). Chemical Compositions of Natural Uraninite. *The Canadian Mineralogist*, *53*(4), 595–622.

Balboni, E., Jones, N., Spano, T., Simonetti, A., & Burns, P. C. (2016). Chemical and Sr isotopic characterization of North America uranium ores: Nuclear forensic applications. *Applied Geochemistry*, *74*, 24–32.

Bonhoure, J., Kister, P., Cuney, M., & Deloule, E. (2007). Methodology for rare earth element determinations of uranium oxides by ion microprobe. *Geostandards and Geoanalytical Research*, *31*(3), 209–225.

Boulyga, S., Konegger-Kappel, S., Richter, S., & Sangely, L. (2015). Mass spectrometric analysis for nuclear safeguards. *Journal of Analytical Atomic Spectrometry*, *30*(7), 1469–1489.

Ciobanu, C. L., Wade, B. P., Cook, N. J., Schmidt Mumm, A., & Giles, D. (2013). Uranium-bearing hematite from the Olympic Dam Cu–U–Au deposit, South Australia: A geochemical tracer and reconnaissance Pb–Pb geochronometer. *Precambrian Research*, *238*, 129–147.

Cui, T., Yang, J., & Samson, I. M. (2012). Tectonic deformation and fluid flow: Implications for the formation of unconformity-related uranium deposits. *Economic Geology*, *107*(1), 147–163.

Cuney, M. (2008). The extreme diversity of uranium deposits. *Mineralium Deposita*, *44*(1), 3.

Cuney, M., Emetz, A., Mercadier, J., Mykchaylov, V., Shunko, V., & Yuslenko, A. (2012). Uranium deposits associated with Na-metasomatism from central Ukraine: A review of some of the major deposits and genetic constraints. *Ore Geology Reviews*, *44*, 82–106.

Cuney, M. & Kyser, K. (Ed.) (2015). *Geology and geochemistry of uranium and thorium deposits*. Short Course Series. Montreal, Quebec: Mineralogical Association of Canada.

Dahlkamp, F. J. (1990). Uranium deposits in collapse breccia pipes in the Grand Canyon region, Colorado Plateau, USA. *Mitteilungen des Naturwissenschaftlichen Vereines für Steiermark*, *120*, 89–98.

Dahlkamp, F. J. (1993). *Uranium ore deposits*. Berlin Heidelberg: Springer-Verlag.

Depiné, M., Frimmel, H. E., Emsbo, P., Koenig, A. E., & Kern, M. (2013). Trace element distribution in uraninite from Mesoarchaean Witwatersrand conglomerates (South Africa) supports placer model and magmatogenic source. *Mineralium Deposita*, *48*(4), 423–435.

Eglinger, A., André-Mayer, A.-S., Vanderhaeghe, O., Mercadier, J., Cuney, M., Decrée, S., … Milesi, J.-P. (2013). Geochemical signatures of uranium oxides in the Lufilian belt: From unconformity-related to syn-metamorphic uranium deposits during the Pan-African orogenic cycle. *Ore Geology Reviews*, *54*, 197–213.

Fayek, M. (2013). Uranium ore deposits: A review. *Uranium: Cradle to Grave*, *43*, 121–147.

Finch, W. I. (1996). *Uranium provinces of North America- their definition, distribution, and models*. Washington, DC: U.S. Geological Survey Bulletin, 2141.

Finch, R., & Murakami, T. (1999). Systematics and paragenesis of uranium minerals. *Reviews in Mineralogy and Geochemistry*, *38*(1), 91–179.

Fisher, L. A., Cleverley, J. S., Pownceby, M., & MacRae, C. (2013). 3D representation of geochemical data, the corresponding alteration and associated REE mobility at the Ranger uranium deposit, Northern Territory, Australia. *Mineralium Deposita*, *48*(8), 947–966.

Fleischer, M., & Altschuler, Z. S. (1969). The relationship of the rare-earth composition of minerals to geological environment. *Geochimica et Cosmochimica Acta*, *33*(6), 725–732.

Forbes, C., Giles, D., Freeman, H., Sawyer, M., & Normington, V. (2015). Glacial dispersion of hydrothermal monazite in the Prominent Hill deposit: An exploration tool. *Journal of Geochemical Exploration*, *156*, 10–33.

Frimmel, H. E., Schedel, S., & Brätz, H. (2014). Uraninite chemistry as forensic tool for provenance analysis. *Applied Geochemistry*, *48*, 104–121.

Fryer, B. J., & Taylor, R. P. (1987). Rare- earth element distributions in uraninites: Implications for ore genesis. *Chemical Geology*, *63*(1), 101–108.

Gaboreau, S., Cuney, M., Quirt, D., Patrier, P., & Mathieu, R. (2007). Significance of aluminum phosphate-sulfate minerals associated with U unconformity-type deposits: The Athabasca basin, Canada. *American Mineralogist*, *92*(2–3), 267–280.

Gao, S., & Wedepohl, K. H. (1995). The negative Eu anomaly in Archean sedimentary rocks: Implications for decomposition, age and importance of their granitic sources. *Earth and Planetary Science Letters*, *133*(1), 81–94.

Hore-Lacy, I. (Ed.) (2016). *Uranium for Nuclear Power: Resources, Mining and Transformation to Fuel*. Elsevier: Woodhead Publishing Series in Energy.

Huston, D. L., Maas, R., Cross, A., Hussey, K. J., Mernagh, T. P., Fraser, G., & Champion, D. C. (2016). The Nolans Bore rare-earth element-phosphorus-uranium mineral system: Geology, origin and post-depositional modifications. *Mineralium Deposita*, *51*(6), 797–822.

IAEA (2009). *World Distribution of Uranium Deposits (UDEPO) with Uranium Deposit Classification*. IAEA TECDOC Series. Vienna: International Atomic Energy Agency.

IAEA (2016). *World Distribution of Uranium Deposits*. Vienna, Austria: IAEA.

Janeczek, J., & Ewing, R. C. (1992). Structural formula of uraninite. *Journal of Nuclear Materials*, *190*, 128–132.

Johnson, J. P., & McCulloch, M. T. (1995). Sources of mineralising fluids for the Olympic Dam deposit (South Australia): Sm–Nd isotopic constraints. *Chemical Geology*, *121*(1–4), 177–199.

Keegan, E., Kristo, M. J., Colella, M., Robel, M., Williams, R., Lindvall, R., … Hutcheon, I. (2014). Nuclear forensic analysis of an unknown uranium ore concentrate sample seized in a criminal investigation in Australia. *Forensic Science International*, *240*, 111–121.

Keegan, E., Richter, S., Kelly, I., Wong, H., Gadd, P., Kuehn, H., & Alonso-Munoz, A. (2008). The provenance of Australian uranium ore concentrates by elemental and isotopic analysis. *Applied Geochemistry*, *23*(4), 765–777.

Keegan, E., Wallenius, M., Mayer, K., Varga, Z., & Rasmussen, G. (2012). Attribution of uranium ore concentrates using elemental and anionic data. *Applied Geochemistry*, *27*(8), 1600–1609.

Lach, P., Mercadier, J., Dubessy, J., Boiron, M.-C., & Cuney, M. (2013). In Situ Quantitative Measurement of Rare Earth Elements in Uranium Oxides by Laser Ablation-Inductively Coupled Plasma-Mass Spectrometry. *Geostandards and Geoanalytical Research*, *37*(3), 277–296.

Lecomte, A., Cathelineau, M., Deloule, E., Brouand, M., Peiffert, C., Loukola-Ruskeeniemi, K., ... Lahtinen, H. (2014). Uraniferous bitumen nodules in the Talvivaara Ni–Zn–Cu–Co deposit (Finland): Influence of metamorphism on uranium mineralization in black shales. *Mineralium Deposita*, *49*(4), 513–533.

Leibold, J. (2013). *Geochemistry and mineralogy of the alteration halo associated with the Three Crow roll-front uranium deposit*. Nebraska, USA: Colorado School of Mines.

Mayer, K., Wallenius, M., & Fanghänel, T. (2007). Nuclear forensic science—from cradle to maturity. *Journal of Alloys and Compounds*, *444*, 50–56.

Mayer, K., Wallenius, M., & Ray, I. (2005). Nuclear forensics—a methodology providing clues on the origin of illicitly trafficked nuclear materials. *Analyst*, *130*(4), 433–441.

Mayer, K., Wallenius, M., & Varga, Z. (2015). Interviewing a Silent (Radioactive) Witness through Nuclear Forensic Analysis. *Analytical Chemistry*, *87*(23), 11605–11610.

Mazumder, R. (2005). Proterozoic sedimentation and volcanism in the Singhbhum crustal province, India and their implications. *Sedimentary Geology*, *176*(1–2), 167–193.

McDonough, W. F., & Sun, S.-S. (1995). The composition of the Earth. *Chemical geology*, *120*(3), 223–253.

Mercadier, J., Cuney, M., Lach, P., Boiron, M. C., Bonhoure, J., Richard, A., ... Kister, P. (2011). Origin of uranium deposits revealed by their rare earth element signature. *Terra Nova*, *23*(4), 264–269.

Oreskes, N., & Einaudi, M. T. (1990). Origin of rare earth element-enriched hematite breccias at the Olympic Dam Cu-U-Au-Ag deposit, Roxby Downs, South Australia. *Economic Geology*, *85*(1), 1–28.

Pal, D. C., Chaudhuri, T., McFarlane, C., Mukherjee, A., & Sarangi, A. K. (2011). Mineral Chemistry and In Situ Dating of Allanite, and Geochemistry of Its Host Rocks in the Bagjata Uranium Mine, Singhbhum Shear Zone, India—Implications for the Chemical Evolution of REE Mineralization and Mobilization. *Economic Geology*, *106*(7), 1155–1171.

Plant, J. A., Simpson, P. R., Smith, B., & Windley, B. F. (1999). Uranium ore deposits; products of the radioactive Earth. *Reviews in Mineralogy and Geochemistry*, *38*(1), 255–319.

Plasil, J. (2014). Oxidation-hydration weathering of uraninite: The current state-of-knowledge. *Journal of Geosciences*, *59*(2), 99–114.

Rai, A.K., Zakaulla, S., & Chaki, A. (2009). Proterozoic stratabound carbonate rock (dolostone) hosted uranium deposits in Vempalle Formation in Cuddapah basin, India (IAEA-CN--175). International Atomic Energy Agency (IAEA).

Roberts, D. E., & Hudson, G. R. T. (1983). The Olympic Dam copper-uranium-gold deposit, Roxby Downs, South Australia. *Economic Geology*, *78*(5), 799–822.

Skirrow, R. G., Jaireth, S., Huston, D., Bastrakov, E., Schofield, A., Van der Wielen, S., & Barnicoat, A. (2009). Uranium mineral systems: Processes, exploration criteria and a new deposit framework. *Geoscience Australia Record*, *20*(2009), 44.

Sørrensen, H. (1992). Agpaitic nepheline syenites: A potential source of rare elements. *Applied Geochemistry*, *7*(5), 417–427.

Takahashi, Y., Yoshida, H., Sato, N., Hama, K., Yusa, Y., & Shimizu, H. (2002). W-and M-type tetrad effects in REE patterns for water–rock systems in the Tono uranium deposit, central Japan. *Chemical Geology*, *184*(3), 311–335.

Tallarico, F. H. B., Figueiredo, B. R., Groves, D. I., Kositcin, N., McNaughton, N. J., Fletcher, I. R., & Rego, J. L. (2005). Geology and SHRIMP U-Pb Geochronology of the Igarapé Bahia Deposit, Carajás Copper-Gold Belt, Brazil: An Archean (2.57 Ga) Example of Iron-Oxide Cu-Au-(U-REE) Mineralization. *Economic Geology*, *100*(1), 7–28.

Varga, Z., Krajkó, J., Peńkin, M., Novák, M., Eke, Z., Wallenius, M., & Mayer, K. (2017). Identification of uranium signatures relevant for nuclear safeguards and forensics. *Journal of Radioanalytical and Nuclear Chemistry*, *312*(3), 639–654.

Varga, Z., Wallenius, M., & Mayer, K. (2010). Origin assessment of uranium ore concentrates based on their rare-earth elemental impurity pattern. *Radiochimica Acta International Journal for Chemical Aspects of Nuclear Science and Technology*, *98*(12), 771–778.

Wülser, P.-A., Brugger, J., Foden, J., & Pfeifer, H.-R. (2011). The Sandstone-Hosted Beverley Uranium Deposit, Lake Frome Basin, South Australia: Mineralogy, Geochemistry, and a Time-Constrained Model for Its Genesis. *Economic Geology*, *106*(5), 835–867.

Zhang, L., Liu, C., Fayek, M., Wu, B., Lei, K., Cun, X., & Sun, L. (2017). Hydrothermal mineralization in the sandstone–hosted Hangjinqi uranium deposit, North Ordos Basin, China. *Ore Geology Reviews*, *80*, 103–115.

## SUPPORTING INFORMATION

Additional Supporting Information may be found online in the supporting information tab for this article.

**Figure S1**. DTA-CN-REE signatures and associated 1σ standard deviations.

**Figure S2.** DTA-CN-REE analysis of uraninite from the North Ordos Basin deposit (Sandstone).

**Figure S3**. DTA-CN-REE analysis of Olympic Dam uranium ore concentrate (UOC) (Fe-O Breccia Complex, reassigned as Granite Related).

**Figure S4**. DTA-CN-REE analysis of Rossing UOC (Intrusive).

**Figure S5**. DTA-CN-REE analysis of Rio Algom UOC (Quartz-Pebble Conglomerate, combined with intrusive).

**Figure S6**. DTA-CN-REE analysis of Denison UOC (Quartz-Pebble Conglomerate, combined with intrusive).

**Figure S7**. DTA-CN-REE analysis of Milliken UOC (Quartz-Pebble Conglomerate, combined with intrusive).

**Figure S8**. DTA-CN-REE analysis of Anaconda UOC (Sandstone-Tabular).

**Figure S9**. DTA-CN-REE analysis of Straz UOC (Sandstone- Tabular).

**Figure S10**. DTA-CN-REE analysis of Rayrock UOC (Granite-Related).

**How to cite this article:** Spano TL, Simonetti A, Wheeler T, et al. A novel nuclear forensic tool involving deposit type normalized rare earth element signatures. *Terra Nova*. 2017;00:1–12. https://doi.org/10.1111/ter.12275